8.1.2.6 Lomonosovite, innelite, kentrolite and related silicates

The sorosilicates from groups VIIIB11…VIIIB14 are listed in Table 1 [91N1]. In addition, other silicates with crystal structures close to the above will be also presented. The structure of nenadkevichite silicate was analyzed together with that of labunstovites in section 8.1.2.5. A vanadate variety of lomonosovite is also presented in this section.

8.1.2.6.1 Crystal structure. Lattice parameters

Lomonosovite, $Na_5Ti_2O_2(Si_2O_7)(PO_4)$; $Na_5Ti_2O_2(Si_2O_7)(VO_4)$; betalomonosovite

Lomonosovite silicate crystallizes in a triclinic lattice having space group $P\bar{1}$ [71R1]. The structure is based on infinite three-layer packets parallel to (001) - Fig. 1a. The $Na(PO_4)$ component is situated in holes between layer packets.

The *vanadium variety of lomonosovite* $Na_5Ti_2O_2[Si_2O_7](VO_4)$ crystallizes in a triclinic structure having P space group [00M1]. The structure may be described as built by seidozerite modules of composition $Na_2Ti_2O_2Se_2O_7$, brucite-type layers of $[TiO_6]$ and $[NaO_6]$ octahedra embedded between layers of $[TiO_6]$ octahedra, $[Si_2O_7]$ groups and $[NaO_8]$ polyhedra. These almost centrosymmetrical triple-layers alternate along the ***c***-axis with polar double-layer modules of composition Na_3VO_4 formed by isolated $[VO_4]^{3-}$ anions and six- and four-coordinate Na cations. Four crystallographically independent Ti atoms in the structure are in an octahedral environment. The structure contains two independent disilicate moieties. One tetrahedron in each disilicate group is smaller. The quasi-isolated "orthovanadate" $[VO_4]$ tetrahedra are distorted. Four of ten crystallographically independent Na atoms are in tetrahedral coordination. Two of the Ti octahedra and two of the Na octahedra form brucite-like layers of edge sharing octahedra parallel to the (*ab*) plane typical for the crystal structures of the lomonosovite group. The cation distribution over the octahedral voids in the synthetic vanadium compound is the same as in lomonosovite. In both cases chains of Ti octahedra alternate with condensed chains of larger Na octahedra in the ***b*** direction [00M1]. From both sides along ***c***-axis ($z \cong 0.2$ and 0.8) these cationic layers are "imprisoned" by complex layers of $[TiO_6]$ octahedra and disilicate groups sharing O vertices combined with Na eight-coordinate polyhedra. That leads to the formation of neutral $Na_2Ti_2O_2[Si_2O_7]$ units – triple-layer blocks parallel to the (*ab*) plane - Fig. 2a. The same centrosymmetrical triple-layer units form the crystal structure of seidozerite where they are linked along the ***c***-axis by an additional center of symmetry through the shared edges of (Zr,Ti) octahedra [90E1, 00M1]. In the subsequent layers ($z \cong 0.4$ and 0.6) of $Na_5Ti_2O_2[Si_2O_7](VO_4)$ the VO_4 tetrahedra are arranged together with $[NaO_4]$ tetrahedra and strongly distorted $[NaO_6]$ octahedra. They are not linked to each other, thus forming orthovanadate groups. In contrast to the quasi-centrosymmetric triple layers around $z = 0$, this "Na_3VO_4" double layer is polar, the tops of the $[VO_4]^{3-}$ anions pointing to the right in both layers [00M1] - Fig. 2b. This is the main difference to the centrosymmetrical structures ($P\bar{1}$ space group) of lomonosovite [71R1].

From the minerals of the lomonosovite group the closest is *betalomonosovite*, the individuality of which is due to the specific position of the P tetrahedra in space. Structural determination [75R1, 86R1] corrected the previous model of the betalomonosovite structure [65K2, 66K1]. The structure, as that of lomonosovite, is based on infinite three-layer packets parallel to (001) - Fig. 1b [86R1]. The bonding of the packets to one another is characteristic for each mineral of the group. In betalomonosovite it is realized by phosphorus and sodium atoms and hydrogen bonds of OH groups. The packets consists of titanium, silicon-oxygen and sodium polyhedra. In the central layer along the *x*-axis are stretched brookite (TiO_2) columns formed from Ti1,2 octahedra, which are similar in dimensions and can be statistically populated also by Fe^{3+} atoms (about 0.3 atoms per unit cell). In the "chain mail" there are Ti3,4 octahedra which are also similar in dimensions. In Ti3 and Ti4 sites are statistically disposed all the "heaviest" isomorphic impurities (Nb, Zr, Mn) of about 0.9 atoms per unit cell [62G2]. The P1,2 tetrahedra lying between the packets cooperate in rudimentary "chains" (through the means of H atoms), which are a distinctive feature of the structure. The P3 atoms supplementing P1 are located at a distance of ~ 0.7 Å and, together with O27 and O28 atoms, form a tetrahedron, oriented similarly to that of lomonosovite [71R1]. The occupancy of the position P3, like the O atoms bound to it, is 20 %. The missing 0.2 P atoms (as compared with chemical analysis) occupy some intermediate positions with low occupancy. There are ten Na positions - Table 2 and Fig. 1b, c. The Ti columns in the central part of the packet are joined together by Na atoms, which are disposed in polyhedra of two types: Na1 octahedra and Na2 five-vertex polygons. As in murmanite [86R2], these

positions are statistically occupied (cannot be simultaneously occupied). The eight vertex polyhedra of the Na3,4 atoms lie in the peripherial layers of the packet, joining the Ti3,4 octahedra along the *y*-axis. In contrast to murmanite, in the networks of which a deficit of sodium is compensated by impurity of the heavy elements, in betalomonosovite the impurities are distributed over titanium positions, while the sodium positions are either occupied by Na, K and Ca, or remain vacant. As a result, Si diorthogroups, "tensed" on homotypic Na3,4 polyhedra, are less distorted than in murmanite. The remaining sodium atoms (Na5-10), fill the space between packets - Fig. 1a. The population of these positions varies from 20 % to 85 %. The most occupied positions correspond to atoms Na6 and Na7. In the pair (Na5 and Na8), the occupancy is below 50 %. The least populated (20 %) are the Na9 and Na10 positions. The shortest distances Na8-Na9, Na5-Na4, Na8-Na3 and Na9-Na3 indicate the impossibility of a simultaneous presence of atoms in these positions. The sites Na9 and Na10 are close to the P1 positions and can be occupied simultaneously only with the P3 tetrahedron. Thus, of the four Na atoms contained in the three-layer packet of lomonosovite [71R1], in betalomonosovite 2.3 atoms are preserved and of the six Na atoms in the interpacket space only 2.6 are left. The deficiency of positive charges in the structure of betalomonosovite is compensated both by introduction of isomorphic high-valence cations and by statistical protonization of some phosphate groups. Reduction of the sodium content in comparison with lomonosovite with partial replacement by protons of OH groups is a necessary condition for the "cooperation"of discrete P orthooctahedra in chains. The stability of the structure requires a definite quantity of sodium in the interpacket space, which ensure the bond between the links of the chain and also a bond of the chains between themselves and with the packets. The existence of several varieties of betalomonosovite was suggested differing in the number of inverted P tetrahedra and the degree of population of the Na sites [86R1]. Inversion of P tetrahedra within sufficiently bulky cavities was seen in the structure of monoclinic fosianite [80K1].

The atomic positions are given in Table 2 while in Table 3 the lattice parameters are listed. The unit cell parameters were related to the parameters *A*, *B*, *C*, [75R1] by the expression $\boldsymbol{a} = -\boldsymbol{A}$, $\boldsymbol{b} = \boldsymbol{B}$, $\boldsymbol{c} = \boldsymbol{A} + \boldsymbol{C}$.

Sobolevite, $Na_{14}Ca_2Ti_3MnO_4(Si_2O_7)_2(PO_4)_4$

Sobolevite crystallizes in a monoclinic-type lattice [83K1, 84D2].

Vuonnemite, $Na_5TiNb_2(Si_2O_7)_2O_2F_2{\cdot}2Na_3PO_4$

Vuonnemite crystallizes in a triclinic-type lattice [83R1, 84D1].

Bornemanite, $Na_7BaTi_2NbSi_4O_{17}(PO_4)(F,OH)$

Bornemanite crystallizes in a orthorhombic-type lattice having space group Ibmm or Ibm2 [75M1, 76F1].

Murmanite, $Na_3(Ti,Nb)_4O_4(Si_2O_7)_2{\cdot}4H_2O$

The structure of murmanite was first described by [65K1] and later corrected by [86R2]. The silicate crystallizes in a triclinic lattice having space group P1 [86R2]. As in case of lomonosovite [71R1] and betalomonosovite [75R1], the structure is based on infinite three-layer stacks parallel to (001) - Fig. 3. The pseudoperiodicity in two directions, found in the rotation patterns required doubling of the parameters obtained from autodiffractometer *a*' and *b*' to $A = 2a'$, $B = 2b'$, $C = c$. Then in [86R2] this was changed to a primitive cell of smaller volume associated with lattice constants $a = (A - B)/2$, $b = (A + B)/2$ and $c = C$ [86R2]. The relations between the three cells of murmanite are shown in Fig. 3. As mentioned in case of betalomonosovite, the individuality of each of these silicates is determined by the content of the interstack space. In case of murmanite, Na and P are replaced by water molecules, with the consequence that there is a shortening of the period ***c*** by 2.7 Å and a less strong binding between the stacks. In the transition from lomonosovite to murmanite, marked changes occur also in the stack itself, both in its anion "networks" and in its cation "wall" [86R2]. The middle part of the stack is a plane layer of close-packed (without gaps) octahedra of titanium and sodium. The Ti1-4 octahedra, joined via edges, form brookite (TiO_2) columns extending along the shortest period ***A***. The titanium octahedra of the columns are of the same dimensions and are scarcely suitable for accommodation of any of larger Mn^{2+}. The large cell has 0.3 to 0.5 Mn and consequently this element cannot be located in an independent position. It was suggested that together with Ti, in the population of columns, Fe^{3+} statistically take part (0.3…0.6 atoms per cell). Between the Ti columns, spaced half a translation along ***B***, there are Na columns made of polyhedra of two types. Thus, in the construction of murmanite sheets Na octahedra are present (as in

lomonosovite [71R1]) as well as Na pyramids similar to betalomonosovite [75R1]. Both the octahedral and pyramidal positions of Na1-4 are filled statistically with a probability of 50 %. The Na2 and Na3 cannot be simultaneously occupied. One of the variants of filling of the Na positions in the wall is shown in Fig. 3b [86R2]. The atomic sites are listed in Table 2. The layers against the two sides of the sheet (network, chain mail) retain the architecture of lomonosovite (betalomonosovite): infinite bands of alternating Ti and Na polyhedra extending along ***B***. The Ti5-8 octahedra in the chain mail are similar in size. In Ti7 and Ti8 sites were suggested Nb impurity atoms to be distributed. The Na polyhedra of the network are differentiated in the form and dimensions. The Na5 site has been suggested to be statistically populated by Mn^{2+}, Fe^{2+}, Zr, Nb and to the least degree by Na. The Na 6 and Na7 were reported to have the composition $Na_{0.4}Ca_{0.6}$ and $Na_{0.8}K_{0.2}$, respectively. The Na8 site is essentially of sodium type. The corresponding polyhedron is in contact with the Ti octahedra both of the sheet and the chain-mail only via vertices and has in common an edge with Si tetrahedra of one of the diortho groups. The free vertex of the polyhedron is occupied by H_2O. The diorthogroups Si_2O_7 (four per unit cell) differ by the relative orientation of tetrahedra. The three-layer stacks of murmanite are joined by hydrogen bonds of water molecules, which enter the coordination polyhedra of titanium and sodium positions of the network [86R1].

The decomposition of lomonosovite and its conversion to murmanite was analysed [86R2]. There is preserved the most stable part of the structure, a framework of titanium and silicon-oxygen polyhedra.

Epistolite, $Na_5TiNb_2(Si_2O_7)_2(O,F)_4 \cdot 5H_2O$

The composition of epistolite was recalculated by [83R1].

Innelite, $Na_2Ba_4CaTi_3O_4(Si_2O_7)_2(SO_4)_2$

Innelite crystallizes in a triclinic structure having space group P1 [61K1, 71C1]. The projection of the structure onto the (*xy*) plane is shown in Fig. 4a [71C1]. In the central chlorite (mica) package, which is infinite in two directions, the "cores" - Fig. 4b - consist of Ti+Na+M octahedra joined to each other along their edges to form a continuous wall (analogue to lamprophillite [64W1] - section 8.1.2.5 - or the murmanite - lomonosovite series. In the walls, infinite columns of M+Ti octahedra can be seen along the ***c***-axis. They alternate with pure Na columns. The centers are clothed on both sides in "anionic" armor: titanium-silicon-oxygen planar networks with discrete [Si_2O_7] diorthogroups and TiO_5 hemioctahedra - Fig. 4c. Similar networks have been found in bafertisite (section 8.1.2.5) and the murmanite group (the only difference being that the Ti, playing the "anionic" role in these structures, has the usual octahedral coordination); and also in lamprophillite [67W1] and fresnoite [69M1] – section 8.1.2.3 (in these two silicates five-coordination is characteristic for titanium in the network). In innelite, the Ti atom plays a double role: cationic (in the octahedron in the center of the packet) and anionic (hemioctahedron in the network armor). The mica-like three-layer packets in innelite are separated by large Ba polyhedra - Fig. 4d. These are joined together to make a two-story wall, with the [SO_4] tetrahedra on the mezzanines [71C1]. See Table 2.

Yoshimuraite, $Ba_2TiMn_2(SiO_4)_2(SO_4, PO_4)(OH, Cl)$

Yoshimuraite crystallizes in a triclinic structure, having space group P $\bar{1}$ [61W1].

*
* *

The lomonosovite group of structures have seidozerite building block-sandwiches being made by a central brucite layer and two identical nets of associated [TiO_6] octahedra and [Si_2O_7] groups with Na atoms in the net voids. This kind of blocks are parallel to the (*ab*) planes in all silicates of the group, therefore having similar lattice parameters ($a \cong 5.5$ Å, $b \cong 7.1$ Å) [00M1]. We note that in Table 3, as reported in original papers, the sequence of *a*, *b*, *c* parameters in some cases are changed. We refer in text to those situations in which the sequence is modified in such a way that smaller and intermediate cell dimensions are *a* and *b*. Along the ***c***-axis those seidozerite modules - Fig. 2a - alternate with different other structure fragments, so the *c* parameters vary significantly from ≅ 12 Å (murmanite and epistolite) to ≅ 41 Å (sobolevite) and ≅ 48 Å (bornemanite). The most simple, from the point of view of the inter-block space composition, are the structures of murmanite [89K1] and epistolite where the space along the ***c***-axis (≅ 12 Å) is filled by water molecules. In the case of innelite, seidozerite blocks alternate along $c \cong 14.76$ Å with fragments of the baryte ($BaSO_4$) crystal structure [71C1]. In lomonosovite and vuonnemite the inter-layer space represents blocks picked out from the Na_3PO_4 structures.

According to [90E1] the crystal structures of quadruphite, $Na_2(Ti,Mn,Zr,Nb)_2O_2[Si_2O_7]\cdot Na_5(Ca,Mg)F[PO_4]_2$, polyphite, $Na_2(Ti,Mn,Zr,Nb)_2OF[Si_2O_7]\cdot Na_6Ca_2(Mg,Mn)F_2[PO_4]_3$ and that of sobolevite $Na_2(Ti,Fe,Zr,Nb)_2OF[Si_2O_7]Na_5CaF[PO_4]_2$ can be interpreted as a polysomatic series based on seidozerite structure as one end member and nacaphite Na_2CaPO_4F structure as the other one [00M1]. The various polysomes (quadruphite, polyphite, sobolevite) arise from different ratios and sequences of the seidozerite and nacaphite blocks. In case of $Na_5Ti_2O_2[Si_2O_7](VO_4)$ structure the seidozerite modules alternate along the ***c***-axis with fragments extracted from the β-Na_3VO_4 structure - Fig. 2b (a = 5.57 Å, b = 7.04 Å, c = 12.10 Å) [76O1], as expected from close unit cell parameters in the (*ab*) plane of both structures [00M1] - Table 3.

Queitite, $Zn_2Pb_4(SiO_4)(Si_2O_7)(SO_4)$

Queitite crystallizes in a monoclinic-type lattice having space group $P2_1$ [79K1, 80F1, 80H1]. SiO_4 tetrahedra and Si_2O_7 double tetrahedra are linked by ZnO_4 tetrahedra forming double sheets with five-membered rings. Between these sheets the Pb ions and isolated SO_4 tetrahedra are inserted.

Macquartite, $CuPb_3(CrO_4)SiO_3(OH)_4\cdot 2H_2O$

Macquartite crystallizes in a monoclinic lattice of space group C2/m, C2 or Cm, with C2/m being the most probable one [80W1, 81F1].

Luddenite, $Cu_2Pb_2Si_5O_{14}\cdot 14H_2O$

The luddenite crystallizes in a monoclinic-type structure [82W1].

Kentrolite, $Pb_2Mn_2O_2(Si_2O_7)$; melanotekite, $Pb_2Fe_2O_2(Si_2O_7)$

The crystal structures of kentrolite and melanotekite were initially reported to be orthorhombic, having $C222_1$ space group [62G1]. The X-ray powder diagrams for natural samples [67G1] or synthetic silicates [66I1, 68I1, 79G1] show weak diffraction peaks which are forbidden in the proposed space group. A detailed structure analysis of the kentrolite-melanotekite series was made later on a natural sample[19)] [91M1]. These silicates are orthorhombic holosymmetric having space group Pbcn (subgroup of Cmcm). The $\left[(Mn,Fe)_2^{3+}O_2Si_2O_7\right]$ fraction, the simplest part, is based on $^1_\infty\left[M^{3+}O_4\right]$ edge-sharing octahedral chains parallel to [001]. These octahedra are alternatively *cis* and *trans* with respect to adjacent octahedra, reminiscent of the structure of synthetic $Ca_3Mn_2^{3+}O_2\left[Si_4O_{12}\right]$. It is decorated on both sides by $[Si_2O_7]$ groups that share corners with it and by disordered Pb atoms in PbO_{6+6} coordination. The projection of the structure along [100] is shown in Fig. 5 [91M1]. There is a suggestion of distorted hexagonal closest packing in this direction, and the distortion is considerable. The top faces of the octahedral chains are approximately parallel to {100}, and the tetrahedra have bases that are likewise approximately parallel to {100}. The silicate tetrahedra actually form oligosilicate dimers $[Si_2O_7]$, and a line piercing these pairs through Si–O–Si is parallel to the ***a***-axis. The $6s^2$ Pb^{2+} lone-pair cations are split in an unexpected fashion, and this splitting was the source of the problems in structure solution. The refinements converged to 0.73 Pb1 and 0.27 Pb2, populated in a complementary fashion, with a Pb1-Pb2 separation of 0.56 Å. Noteworthy is the unsymmetrical splitting of Pb atoms. Bond distance averages are $^{[6]}M1^{3+}$–O= 2.01 Å (prolate spheroid), $^{[6]}M2^{3+}$–O = 2.03 Å (oblate spheroid) $^{[4]}$Si–O = 1.63 Å, $^{[6]}$Pb1–O = 2.40…2.99 Å (2.60 Å mean) and $^{[6]}$Pb2–O = 2.27…3.02 Å (2.63 Å mean). Five cations and five anions comprise the asymmetric unit. Dominant $3d^4$ Mn^{3+} at M1 and M2 evidence tetragonal Jahn-Teller distortion of the coordination polyhedra as elongated (prolate) and compressed (oblate) octahedra, respectively [91M1].

Fosinaite, $Na_3CaPSiO_7$

The fosinaite, $Na_3CaPSiO_7$, crystallizes in a monoclinic structure having space group P2/c [74K1, 80K1]. The structure of $Na_3(Ca,Ce)PSiO_7$ silicate is orthorhombic with space group $P22_12$ or $P22_12_1$ [74K1]. The cationic part of the monoclinic structure is concentrated in geometrically similar sheets perpendicular to [100]. Chains of Ca polyhedra, constricted by pairs of Na polyhedra, are distinguished in the sheets at the $x \cong 0$ level; at the $x \cong 0.5$ level the sheets are composed of Na polyhedra. The cation framework is penetrated by the anion framework,

in which there are combined tubular columns of four rings of two types: silicon-oxygen rings [SiO_4] and mixed rings of P orthotetrahedra and Na polyhedra. The tetrahedral four-membered [Si_4O_{12}] rings are adapted to specific characteristics of the cation arrangements, accounting for the change in their proper symmetry [80K1]. The combinated anion arrangement (consisting of two types of tetrahedra – Si and P) brings monoclinic fosinaite close to lomonosovite [71R1] and innelite [71C1]. However, in contrast with these silicates, fosinaite exhibits similar functions of the phosphate and silicate tetrahedra (these tetrahedra are of four-membered rings). In lomonosovite and innelite the tetrahedra not only differ in the central cations but also play different roles. Both of the latter structures are characterized by stacks consisting of cation cores with anion "chain mail' – titanium-silicon-oxygen lattice with [Si_2O_7] diortho groups and Ti polyhedra. The space between the stacks contains [PO_4] orthotetrahedra and Na cations (lomonosovite) or [SO_4] orthotetrahedra and Ba cations (innelite) [80K1].

The lattice parameters of the silicates discussed above are listed in Table 3.

8.1.2.6.2 Optical properties

Kentrolites

The infrared (IR) spectra for ^{28}Si–^{30}Si isotopic species $Pb_2In_2Si_2O_9$ are shown in Fig. 6 while the Raman spectrum of $Pb_2Sc_2Si_2O_9$ is reproduced in Fig. 7 [79G1]. The IR spectrum may be analysed by considering two regions: (a) the low frequency region (650…300 cm^{-1}) where the spectrum strongly depends of the nature of the trivalent cation M^{3+}. This part of the spectrum is of complex origin with contributions from both Si_2O_7 bending vibrations and lattice vibrations; (b) a higher frequency region (650…1050 cm^{-1}) in which the various kentrolites exhibit a similar pattern with large (up to 13 cm^{-1}) ^{28}Si–^{30}Si isotopic shifts for some bands at least. These bands are related to stretching vibrations of Si–O bonds, and in addition , the general pattern is characteristic of the pyrosilicate group. The symmetric (ν_{sym}) and antisymmetric (ν_{as}) frequencies of the Si–O–Si bridge have been identified analysing the ^{28}Si–^{30}Si isotopic shifts. The frequency range 630…730 cm^{-1} and the band observed near 700 cm^{-1} were assigned to bridge symmetric stretch and characterized by large isotopic shift. This mode appears in both IR and Raman spectra. The IR band located near 1000 cm^{-1} was assigned to the bridge antisymmetric stretch. There is no equivalent peak in the Raman spectrum (is possibly very weak). The vibrations of terminal SiO_3 groups were roughly classified as symmetric or antisymmetric with respect to the local ternary axis of the SiO_3 group. The 830…850 cm^{-1} band in the IR spectrum which is missing or is weak in the Raman spectrum, was assigned to the symmetrical out-of-phase vibration, ν_{sym}. The corresponding in phase vibrations, ν_{sym}, was attributed to 885…900 cm^{-1} band, which appears in both IR and Raman spectra. The higher-frequency bands (900…960 cm^{-1}) were assigned to the antisymmetric stretching motions, ν_{as}, as a whole. There was no possibility to discriminate between in-phase and out-of-phase vibrations. A linear relation was shown as function of the ionic radius of trivalent cations in $Pb_2M_2^{3+}Si_2O_9$ kentrolites for the bridge-stretching frequencies written as $(\nu_{as} - \nu_{sym}) / (\nu_{as} + \nu_{sym})$ - Fig. 8. Acoording to [79G1], the increase of the difference $\nu_{as} - \nu_{sym}$ with ionic radius of M^{3+} cations is probably related to an increase of the bridge angle when the size of the trivalent cation increase.

*
* *

The refractive indices of some silicates are listed in Table 4.

Tables and figures

Table 1. Sorosilicates from groups VIIIB11 – VIIIB14 [91N1].

Silicate	Composition	Group
Lomonosovite	$Na_5Ti_2O_2(Si_2O_7)(PO_4)$ $Na_5Ti_2O_2(Si_2O_7)(VO_4)$	VIIIB11
Sobolevite	$Na_{14}Ca_2Ti_3MnO_4(Si_2O_7)_2(PO_4)_4$	VIIIB11
Vuonnemite	$Na_5TiNb_2(Si_2O_7)_2O_2F_2 \cdot 2Na_3PO_4$	VIIIB11
Bornemanite	$Na_7BaTi_2NbSi_4O_{17}(PO_4)(F,OH)$	VIIIB11
Murmanite	$Na_3(Ti,Nb)_4O_4(Si_2O_7)_2 \cdot 4H_2O$	VIIIB11
Epistolite	$Na_5TiNb_2(Si_2O_7)_2(O,F)_4 \cdot 5H_2O$	VIIIB11
Nenadkevichite	$Na(Nb,Ti)Si_2O_6(O,OH) \cdot 2H_2O$	VIIIB11
Innelite	$Na_2Ba_4CaTi_3O_4(Si_2O_7)_2(SO_4)_2$	VIIIB12
Yoshimuraite	$Ba_2TiMn_2(SiO_4)_2(SO_4,PO_4)(OH,Cl)$	VIIIB12
Queitite	$Zn_2Pb_4(SiO_4)(Si_2O_7)(SO_4)$	VIIIB13
Macquartite	$CuPb_3(CrO_4)SiO_3(OH)_4 \cdot 2H_2O$	VIIIB13
Luddenite	$Cu_2Pb_2Si_5O_{14} \cdot 14H_2O$	VIIIB13
Creaseyite	$Cu_2Pb_2(Fe,Al)_2Si_5O_{17} \cdot 6H_2O$	VIIIB13
Kentrolite	$Pb_2Mn_2(Si_2O_7)O_2$	VIIIB14
Melanotekite	$Pb_2Fe_2O_2(Si_2O_7)$ $Pb_2M_2O_2(Si_2O_7)$ M = Cr,Mn, Sc, In, Ga, MgSn, CoSn, etc.	VIIIB14
Molybdophyllite	$Mg_2Pb_2Si_2O_7(OH)_2$	VIIIB14
Fosinaite	$Na_3CaPSiO_7$	

Table 2. Atomic coordinates, isotropic thermal parameters and population.

a) Lomonosovite having triclinic structure, space group $P\bar{1}$ [71R1].

Atom	*x*	*y*	*z*
Ti1	0.781	0.612	0.007
Ti2	0.053	0.923	0.216
P	0.256	0.223	0.433
Si1	0.508	0.200	0.179
Si2	0.555	0.638	0.198
Na1	0.769	0.120	0.008
Na2	0.054	0.416	0.227
Na3	0.683	0.975	0.359
Na4	0.722	0.460	0.398
Na5	0.184	0.738	0.415
O1	0.500	0.612	0.083
O2	0.977	0.429	0.072
O3	0.425	0.200	0.067
O4	0.956	0.834	0.092
O5	0.763	0.108	0.208
O6	0.538	0.425	0.227
O7	0.825	0.737	0.246
O8	0.275	0.125	0.208

Table 2 (continued)

Atom	*x*	*y*	*z*
O9	0.338	0.752	0.242
O10	0.146	0.022	0.365
O11	0.138	0.396	0.395
O12	0.538	0.221	0.442
O13	0.800	0.773	0.471

b) Betalomonosovite having triclinic lattice, space group $P\bar{1}$ [86R1].

Atom	*x*	*y*	*z*	B_{iso} [Å^2]	Site population
Ti1	0.2311(5)	0.3089(2)	0.0065(3)	1.42	1.0
Ti2	0.7510(5)	0.1859(2)	0.9922(3)	1.55	1.0
Ti3	0.1526(4)	0.4726(2)	0.2203(2)	0.80	1.0
Ti4	0.8496(5)	0.0290(3)	0.7789(2)	1.13	1.0
Si1	0.6333(8)	0.3269(4)	0.1980(4)	1.28	1.0
Si2	0.3534(9)	0.1740(4)	0.7975(4)	1.99	1.0
Si3	0.6502(7)	0.1090(2)	0.1813(2)	1.33	1.0
Si4	0.3455(8)	0.3899(3)	0.8168(3)	2.59	1.0
P1	0.269(2)	0.1239(7)	0.4448(6)	2.35	0.6
P2	0.8408(8)	0.3812(3)	0.5580(3)	2.63	1.0
P3	0.138(6)	0.122(3)	0.435(3)	3.00	0.2
Na1	0.225(2)	0.057(1)	0.010(1)	2.17	0.6
Na2	0.782(3)	0.450(1)	0.986(1)	3.21	0.5
Na3	0.159(2)	0.234(1)	0.258(1)	2.45	0.6
Na4	0.847(2)	0.273(2)	0.745(1)	2.60	0.6
Na5	0.790(4)	0.145(2)	0.608(2)	1.79	0.3
Na6	0.356(2)	0.510(1)	0.624(1)	2.85	0.8
Na7	0.271(2)	0.009(1)	0.628(1)	3.77	0.7
Na8	0.236(4)	0.360(2)	0.396(2)	2.91	0.4
Na9	0.588(4)	0.242(2)	0.397(2)	4.00	0.2
Na10	0.337(5)	0.270(2)	0.602(2)	4.94	0.2
O1	0.901(2)	0.279(1)	0.929(1)	2.30	1.0
O2	0.613(2)	0.099(1)	0.071(1)	2.69	1.0
O3	0.369(3)	0.397(1)	0.936(1)	3.97	1.0
O4	0.136(2)	0.422(1)	0.092(1)	2.64	1.0
O5	0.866(2)	0.085(1)	0.909(1)	2.36	1.0
O6	0.365(2)	0.077(1)	0.212(1)	3.45	1.0
O7	0.554(2)	0.449(1)	0.782(1)	3.80	1.0
O8	0.679(2)	0.223(1)	0.229(1)	3.32	1.0
O9	0.361(2)	0.276(2)	0.765(1)	2.37	1.0
O10	0.392(2)	0.376(1)	0.249(1)	2.94	1.0
O11	0.566(2)	0.112(1)	0.749(1)	2.57	1.0
O12	0.868(2)	0.053(1)	0.217(1)	2.52	1.0
O13	0.058(2)	0.421(1)	0.787(1)	3.15	1.0
O14	0.879(2)	0.395(1)	0.246(1)	3.02	1.0
O15	0.080(2)	0.125(1)	0.759(2)	2.53	1.0

Table 2 (continued)

Atom	*x*	*y*	*z*	B_{iso} [Å^2]	Site population
O16	0.186(2)	0.027(1)	0.372(1)	2.68	1.0
O17	0.794(3)	0.468(2)	0.626(2)	4.95	1.0
O18	0.577(2)	0.300(2)	0.082(1)	2.36	1.0
O19	0.801(4)	0.296(1)	0.600(2)	6.71	0.95
O20	0.566(4)	0.118(2)	0.461(2)	2.45	0.4
O21	0.119(3)	0.375(1)	0.540(2)	7.69	1.0
O22	0.665(4)	0.384(1)	0.466(1)	4.98	0.8
O23	0.166(3)	0.126(1)	0.537(1)	4.93	0.85
O24	0.244(3)	0.220(2)	0.415(2)	4.13	0.9
O25	0.410(2)	0.193(1)	0.916(1)	2.57	1.0
O26	0.073(2)	0.211(1)	0.071(1)	1.87	1.0
O27	0.892(6)	0.121(3)	0.471(2)	3.04	0.2
O28	0.343(13)	0.098(5)	0.531(6)	5.00	0.2

c) Murmanite having triclinic structure, space group P1 [86R2].

Atom	*x*	*y*	*z*	B_{iso} [Å^2]
Ti1	0.683	0.551	0.994	1.10
Ti2	0.165	0.069	0.001	1.28
Ti3	0.316	0.445	0.981	1.41
Ti4	0.800	0.940	0.983	1.26
Ti5	0.743	0.068	0.721	1.87
Ti6	0.248	0.568	0.717	2.16
Ti7	0.220	0.950	0.271	1.09
Ti8	0.754	0.414	0.258	0.82
Si1	0.142	0.187	0.742	1.64
Si2	0.647	0.687	0.742	1.57
Si3	0.143	0.537	0.222	1.53
Si4	0.823	0.798	0.228	1.28
Si5	0.613	0.009	0.215	0.96
Si6	0.356	0.328	0.228	1.01
Si7	0.344	0.965	0.766	1.89
Si8	0.852	0.466	0.753	2.09
Na1	0.905	0.303	0.988	0.10
Na2	0.069	0.682	0.974	0.63
Na3	0.381	0.805	0.004	1.97
Na4	0.552	0.174	0.986	0.75
Na5	0.983	0.177	0.272	1.37
Na6	0.492	0.313	0.696	1.95
Na7	0.985	0.809	0.705	2.39
Na8	0.480	0.673	0.272	3.73
O1	0.317	0.284	0.088	1.54
O2	0.815	0.764	0.096	1.51
O3	0.984	0.942	0.277	1.12
O4	0.146	0.506	0.077	2.45

Table 2 (continued)

Atom	*x*	*y*	*z*	B_{iso} [Å^2]
O5	0.606	0.967	0.070	1.77
O6	0.730	0.411	0.103	2.74
O7	0.197	0.936	0.114	1.45
O8	0.431	0.004	0.272	0.47
O9	0.225	0.686	0.265	2.94
O10	0.756	0.187	0.254	0.70
O11	0.973	0.100	0.088	2.02
O12	0.992	0.899	0.924	2.30
O13	0.491	0.612	0.074	2.13
O14	0.305	0.491	0.265	0.85
O15	0.522	0.377	0.290	1.57
O16	0.686	0.876	0.275	2.29
O17	0.231	0.193	0.289	0.49
O18	0.508	0.395	0.907	2.07
O19	0.809	0.639	0.292	0.82
O20	0.159	0.243	0.893	1.59
O21	0.224	0.328	0.696	3.85
O22	0.993	0.416	0.247	1.53
O23	0.517	0.051	0.718	3.69
O24	0.014	0.540	0.725	4.30
O25	0.270	0.571	0.879	1.47
O26	0.692	0.852	0.697	4.28
O27	0.771	0.083	0.892	3.15
O28	0.211	0.026	0.714	3.86
O29	0.502	0.549	0.711	3.48
O30	0.947	0.141	0.712	2.16
O31	0.673	0.733	0.906	2.28
O32	0.342	0.995	0.915	2.43
O33	0.856	0.505	0.899	1.98
O34	0.315	0.769	0.722	1.94
O35	0.816	0.634	0.726	2.72
O36	0.817	0.274	0.721	3.06
$(H_2O)_1$	0.249	0.982	0.459	3.16
$(H_2O)_2$	0.775	0.446	0.460	2.59
$(H_2O)_3$	0.998	0.230	0.453	3.73
$(H_2O)_4$	0.473	0.767	0.451	1.95
$(H_2O)_5$	0.988	0.762	0.521	4.12
$(H_2O)_6$	0.500	0.255	0.505	2.80
$(H_2O)_7$	0.691	0.054	0.534	3.34
$(H_2O)_8$	0.208	0.547	0.536	2.97

Table 2 (continued)

d) Innelite having triclinic-type structure [71C1].

Atom	*x*	*y*	*z*
Ba1	0	0	0
Ba2	0.299	0.293	0.0624
Ba3	0.0784	0.537	0.513
Ba4	0.302	0.842	0.575
Ti1	0.488	0.368	0.602
Ti2	0.677	0.916	0.319
Ti3	0.889	0.480	0.976
Si1	0.495	0.652	0.108
Si2	0.500	0.0791	0.0982
Si3	0.877	0.195	0.473
Si4	0.875	0.760	0.474
T1(S1)	0.204	0.705	0.045
T2(S2)	0.164	0.122	0.528
M	0.678	0.149	0.784
Na1	0.681	0.423	0.270
Na2	0.677	0.662	0.761
O1	0.452	0.858	0.106
O2	0.610	0.895	0.606
O3	0.919	0.295	0.233
O4	0.447	0.542	0.845
O5	0.0957	0.689	0.0458
O6	0.918	0.288	0.733
O7	0.771	0.445	0.952
O8	0.763	0.742	0.452
O9	0.125	0.212	0.767
O10	0.129	0.217	0.295
O11	0.130	0.919	0.558
O12	0.264	0.150	0.561
O13	0.234	0.615	0.284
O14	0.238	0.619	0.833
O15	0.244	0.919	0.0721
O16	0.917	0.675	0.233
O17	0.919	0.686	0.741
O18	0.599	0.407	0.605
O19	0.451	0.172	0.867
O20	0.453	0.148	0.348
O21	0.450	0.538	0.333
O22	0.915	0.994	0.495
O23	0.767	0.127	0.444
O24	0.600	0.114	0.127
O25	0.607	0.683	0.108
O26	0.752	0.919	0.0167

Table 2 (continued)

e) Kentrolite having orthorhombic structure, space group Pbcn (subgroup of Cmcm) [91M1].

Atom	Site population	Equipoint rank number	*x*	*y*	*z*	B_{iso} [Å^2]
Pb1	0.73(2)	8	0.4561(1)	0.3012(1)	0.5500(1)	0.93
Pb2	0.27(2)	8	0.5351(22)	0.3098(3)	0.5475(2)	1.07
M1	1.00	4	1/2	0	0	0.58
M2	1.00	4	1/2	0.1482(2)	1/4	0.57
Si	1.00	8	0.2140(4)	–0.0907(3)	0.2528(4)	0.50
O1	1.00	8	0.3402(12)	0.0054(8)	0.3361(8)	0.74
O2	1.00	8	0.2995(15)	–0.1135(8)	0.1031(9)	1.11
O3	1.00	8	0.1888(13)	–0.2217(8)	0.3272(9)	0.91
O4	1.00	4	0	–0.0286(13)	1/4	1.88
O5	1.00	8	0.6094(13)	0.1442(7)	0.4227(8)	0.63

Table 3. Crystal structures and lattice parameters at RT.

Silicate	Space group	Lattice parameters				Refs.
		a [Å]	*b* [Å]	*c* [Å]	α, β, γ	
Lomonosovite $Na_5Ti_2[Si_2O_7][PO_4]O_2$	$P\bar{1}$	5.44	7.163	14.83	$\alpha = 99°$ $\beta = 106°$ $\gamma = 90°$	71R1
$Na_5Ti_2[Si_2O_7][VO_4]O_2$	P	5.309(1)	7.133(1)	14.746(2)	$\alpha = 99.05(1)°$ $\beta = 95.97(1)°$ $\gamma = 90.08(1)°$	00M1
Betalomonosovite[1)]	$P\bar{1}$	5.326(2)	14.184(3)	14.47(2)	$\alpha = 102.2(1)°$ $\beta = 95.5(1)°$ $\gamma = 90.17(2)°$	86R1
Sobolovite[2)]	monoclinic	7.074(1)	5.4087(3)	40.606(9)	$\beta = 93.18°$	83K1, 84D2
Vuonnemite[3)]	triclinic	5.501(1)	7.162(1)	14.440(1)	$\alpha = 92.63(1)°$ $\beta = 95.33(1)°$ $\gamma = 90.57(1)°$	83R1, 84D1
Bornemanite[4)]	Ibmm or Ibm2	5.48(5)	7.10(5)	48.2(1)		75M1, 76F1
Murmanite[5)]	P1	8.700(5)	8.728(4)	11.688(14)	$\alpha = 94.31(6)°$ $\beta = 98.62(8)°$ $\gamma = 105.62(3)°$	86R2
Innelite[6)]	triclinic	5.38(2)	7.14(3)	14.76(10)	$\alpha \cong 90°$ $\beta \cong 95°$ $\gamma \cong 90°$	61K1
Innelite[7)]	P1	14.76	7.14	5.38	$\alpha = 99°$ $\beta = 95°$ $\gamma = 99°$	71C1
Yoshimuraite[5)]	$P\bar{1}$	7.00(1)	14.71(2)	5.39(1)	$\alpha = 93.5(2)°$ $\beta = 90.2(2)°$ $\gamma = 95.3(2)°$	61W1

Table 3 (continued)

Silicate	Space group	Lattice parameters				Refs.
		a [Å]	*b* [Å]	*c* [Å]	α, β, γ	
Queitite[8)]	$P2_1$	11.362(3)	5.266(1)	12.655(3)	$\beta = 108.16(2)°$	79K1, 80F1,80H1
Macquartite[9)]	C2/m,C2 or Cm	20.81	5.84	9.26	$\beta = 91°48'$	80W1, 81F1
Luddenite[10)]	monoclinic	7.85	20.06	10.72	$\beta = 90.78°$	82W1
Kentrolite[5)]	orthorhombic	7.00	11.04	9.97		67G1
$Pb_2Fe_2Si_2O_9$		6.93(1)	10.98(2)	10.06(2)		66I1
$Pb_2Fe_2Si_2O_9$[11)]		6.972(3)	10.990(4)	10.043(5)		79G1
$Pb_2Mn_2Si_2O_9$		6.98(1)	11.04(2)	9.96(2)		66I1
$Pb_2Mn_2Si_2O_9$[12)]		6.986(6)	11.027(9)	9.995(9)		79G1
$Pb_2Cr_2Si_2O_9$		6.88(1)	10.84(2)	10.01(2)		68I1
$Pb_2Cr_2Si_2O_9$[11)]		6.882(2)	10.827(3)	9.994(2)		79G1
$Pb_2Sc_2Si_2O_9$		7.00(1)	11.30(2)	10.44(2)		68I1
$Pb_2Sc_2Si_2O_9$[12)]		7.000(4)	11.278(5)	10.414(4)		79G1
$Pb_2In_2Si_2O_9$		7.02(1)	11.39(2)	10.54(2)		68I2
$Pb_2In_2Si_2O_9$[12)]		7.006(2)	11.365(3)	10.541(3)		79G1
$Pb_2Ga_2Si_2O_9$		6.95(1)	10.90(2)	9.91(2)		68I1
$Pb_2MgSnSi_2O_9$[13)]		6.970(2)	11.179(3)	10.217(2)		79G1
$Pb_2CoSnSi_2O_9$[14)]		6.964(1)	11.178(2)	10.261(2)		79G1
$Pb_2NiSnSi_2O_9$[15)]		6.970(2)	11.125(3)	10.197(2)		79G1
$Pb_2CuSnSi_2O_9$[16)]		6.975(2)	11.228(3)	10.129(2)		79G1
$Pb_2CoTiSi_2O_9$[17)]		6.897(3)	11.025(3)	10.102(2)		79G1
$Pb_2NiTiSi_2O_9$[18)]		6.915(3)	10.983(3)	10.048(3)		79G1
Melanotekite[5)]	orthorhombic	6.97	11.00	9.93		67G1
Kentrolite[19)]	Pbcn	6.961(2)	11.018(3)	9.964(5)		91M1
Fosinaite[20)]	P2/c	7.303(2)	12.201(5)	14.715(4)	$\beta = 91.93°$	74K1, 80K1
Fosinaite[21)]	$P22_12$ or $P22_12_1$	12.23	14.62	7.21		74K1, 80K1

[1)] $[(Ti_{1.7}Fe^{3+}_{0.3})Na_{1.1}O_4][(Ti_{1.3}Nb_{0.3}Zr_{0.15}Mn^{2+}_{0.2}Mg_{0.05})(Na_{1.2}Ca_{0.1}K_{0.2})(Si_2O_7)_2][Na_{2.6}(H_2PO_4)_2]$;
[2)] $Na_{13.47}(Ca_{1.60}Mg_{0.21})(Mn_{0.79}Fe_{0.11})(Ti_{2.67}Nb_{0.46})P_{3.94}Si_{4.00}(O_{33.19}F_{0.52})$;
[3)] natural sample, $Na_5TiNb_2(Si_2O_7)_2 \cdot 2Na_3PO_4 \cdot F \cdot 1.5O_2$;
[4)] $BaNa_4Ti_2NbSi_4O_{17}(F,OH)1Na_3PO_4$;
[5)] natural sample;
[6)] $(Ba_{3.69}K_{0.20}Ca_{0.16}Na_{0.03})(Ti_{2.96}Al_{0.06}Fe^{3+}_{0.11}Fe^{2+}_{0.10}Mg_{0.27}Mn_{0.19})Si_4O_{18}(OH,F)_{1.5} \cdot 1.15Na_2SO_4$;
[7)] $Na_{2.33}Ca_{0.16}Mg_{0.27}Fe_{0.2}(Ba,K,Mn)_4(Ti,Al)_3Si_4O_{24}(OH,F)_2 \cdot 1.15S$;
[8)] $Pb_{3.87}Zn_{2.01}Si_{3.10}S_{0.98}O_{15}$;
[9)] $Pb_3Cu(CrO_4)SiO_3(OH)_4 \cdot 2H_2O$;
[10)] $Cu_2Pb_2Si_5O_{14} \cdot 14H_2O$ (slightly different from above);
[11)] synthesis temperature 875 °C;
[12)] synthesis temperature 900 °C;
[13)] synthesis temperature 775…800 °C;
[14)] synthesis temperature 800…900 °C;
[15)] synthesis temperature 925 °C;
[16)] synthesis temperature 750 °C;
[17)] synthesis temperature 800 °C;
[18)] synthesis temperature 775 °C;
[19)] $Pb^{2+}_{1.98}(Mn^{3+}_{1.28}Fe^{3+}_{0.61}Al^{3+}_{0.04}Ti^{4+}_{0.04}Mg^{2+}_{0.01})Si_{2.02}O_9$;
[20)] $Na_3CaPSiO_7$;
[21)] $Na_3(Ca,Ce)PSiO_7$;

Table 4. Refractive indices.

Silicate[a)]	n_α	n_β	n_γ	$2V$			Refs.
				exp.	calc.		
Sobolevite[2)]	1.627(2)	1.686(2)	1.690(2)	25 (red) 29° (yellow) 33° (blue)		biaxial, negative	83K1
Vuonnemite[3)]	1.6360(5)	1.6544(5)	1.6795(5)	86(2)°	82.3°	biaxial, positive	83R1
Bornemanite[4)]	1.682 1.683	1.695 1.687	1.720 1.718	40°	66°	biaxial, positive	75M1
Yoshimuraite[5)]	1.763	1.777	1.785	85°…90°		biaxial, positive	61W1
Innelite[6)]	1.726(1)	1.737(1)	1.766(1)	82(2)°		biaxial, positive	61K1
Innelite[7)]	1.766(1)	1.737(1)	1.726(1)			biaxial, positive	71C1
Queitite[8)]	1.859	1.901	1.903	≅ 90°			79K1, 80F1
Macquartite[9)]	2.28	2.31	2.34	85°		biaxial, negative	80W1, 81F1
Luddenite[10)]	1.852	1.852	1.867		40°	positive	82W1

[a)] the compositions are given in Table 3.

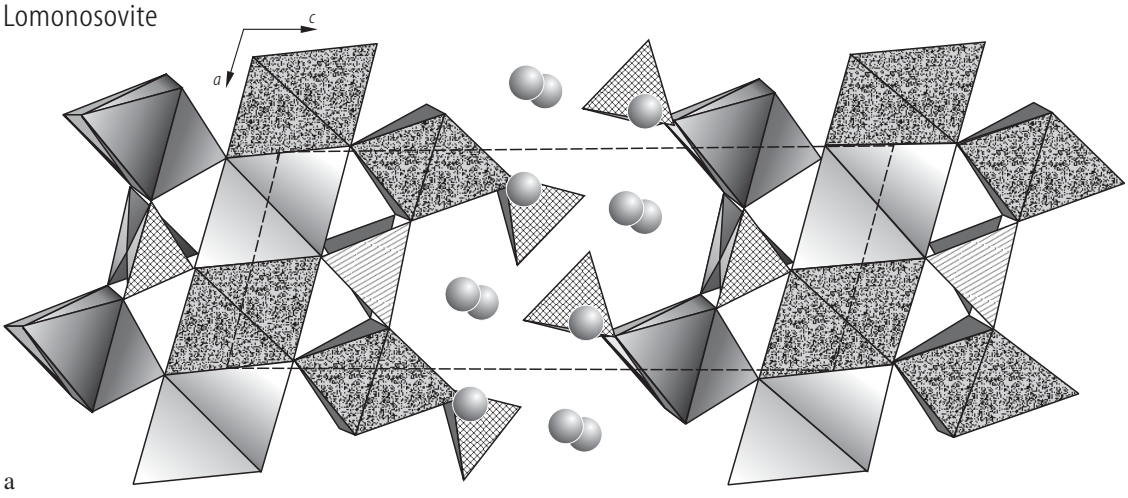

a

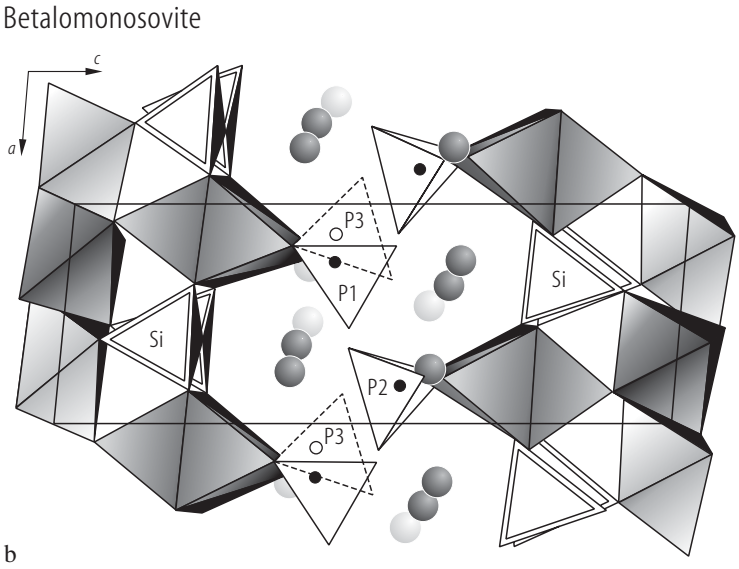

b

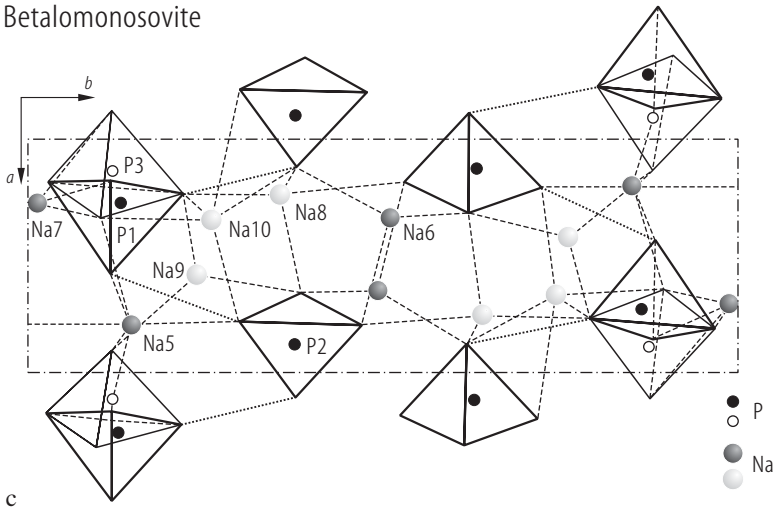

c

Fig. 1. Lomonosovite. **(a)** Projection of the structure in (*ac*) plane. The positions of Na3, Na4 and Na5 atoms are denoted by circles [71R1]; Betalomonosovite: **(b)** projection of structure on (010). White (light) circles mark "lomonosovite" positions of P and Na, dark circles mark "betalomonosovite" positions; **(c)** fragment of betalomonosovite structure in projection of (001). Dashed lines, bonds of Na atoms with P-tetrahedra; dotted lines hydrogen bonds [86R1].

$Na_5Ti_2O_2[Si_2O_7](VO_4)$

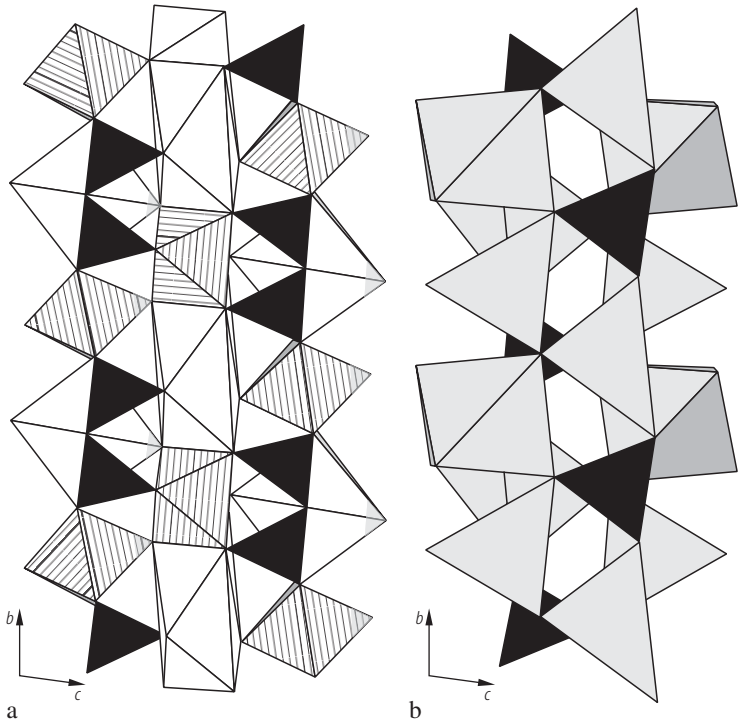

Fig. 2. $Na_5Ti_2O_2[Si_2O_7](VO_4)$. **(a)** Seidozerite module $Na_2Ti_2O_2[Si_2O_7]$in [100] projection. Ti octahedra hatched, Si tetrahedra dark, Na octahedra bright. **(b)** β-Na_3VO_4 module in a [100] projection. $[VO_4]$ tetrahedra dark [00M1].

Murmanite

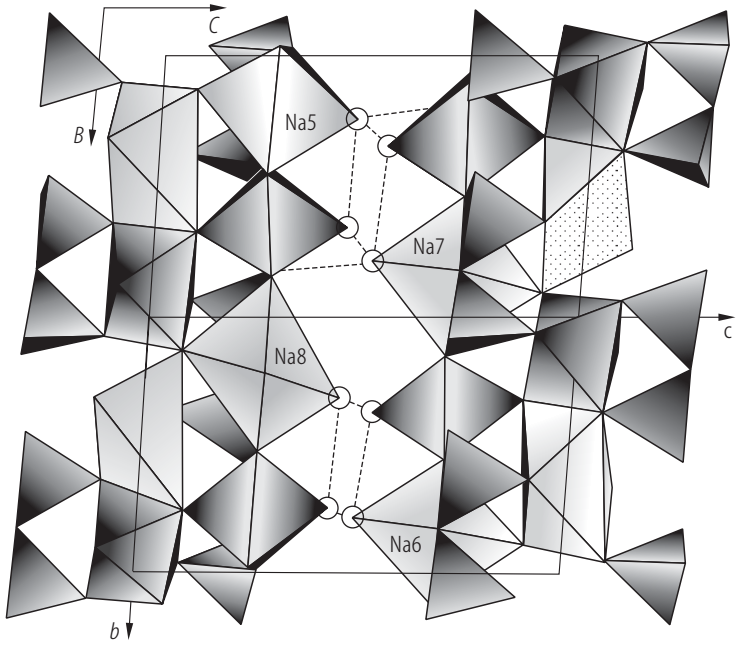

a

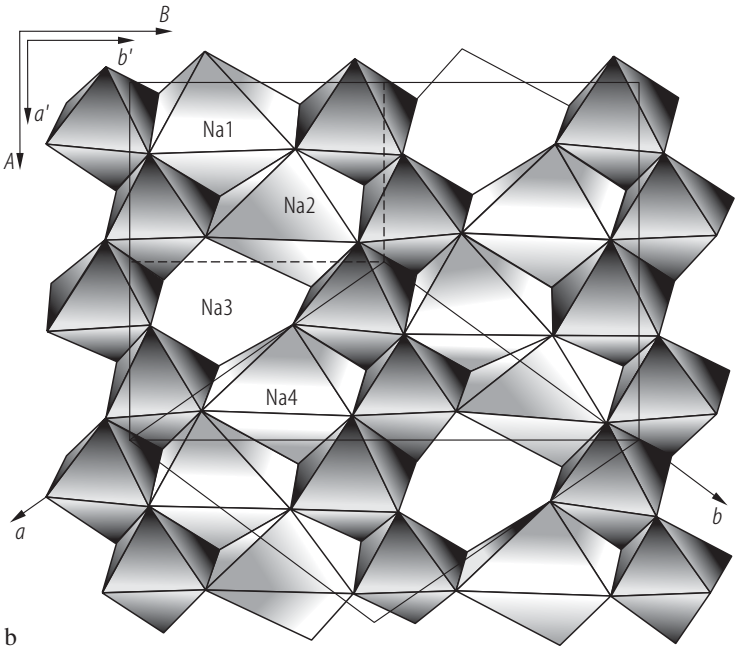

b

Fig. 3. Murmanite. **(a)** Projection of structure on (100). Light and dotted shading marks polyhedra of sodium positions; circles are H_2O molecules; dashed lines are hydrogen bonds; **(b)** cation sheet projected on (001). The crystallochemical analysis is "tied" to the traditional unit cell for minerals of the lomonosovite group with axes *A* and *B* (see text) [86R2].

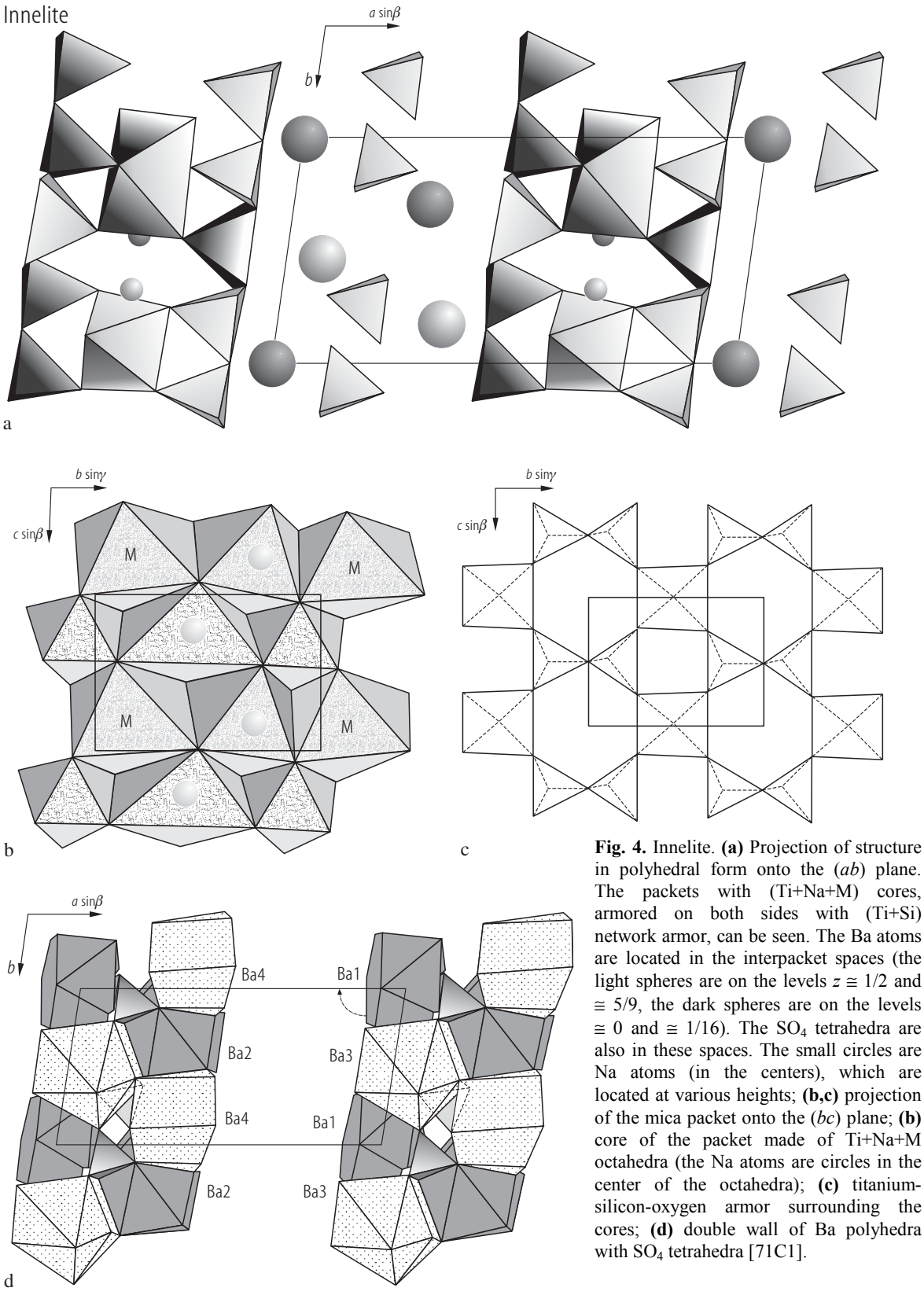

Fig. 4. Innelite. **(a)** Projection of structure in polyhedral form onto the (*ab*) plane. The packets with (Ti+Na+M) cores, armored on both sides with (Ti+Si) network armor, can be seen. The Ba atoms are located in the interpacket spaces (the light spheres are on the levels $z \cong 1/2$ and $\cong 5/9$, the dark spheres are on the levels $\cong 0$ and $\cong 1/16$). The SO_4 tetrahedra are also in these spaces. The small circles are Na atoms (in the centers), which are located at various heights; **(b,c)** projection of the mica packet onto the (*bc*) plane; **(b)** core of the packet made of Ti+Na+M octahedra (the Na atoms are circles in the center of the octahedra); **(c)** titanium-silicon-oxygen armor surrounding the cores; **(d)** double wall of Ba polyhedra with SO_4 tetrahedra [71C1].

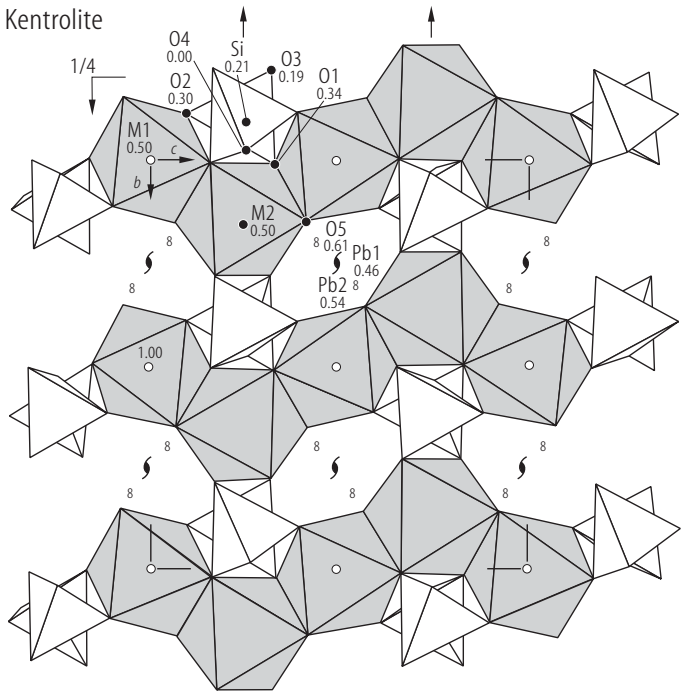

Fig. 5. Kentrolite. Polyhedral representation of the crystal structure projected along [100]. The Pb centroids are small circles. Heights are in fractional coordinates (x). Some symmetry elements are drawn in [91M1].

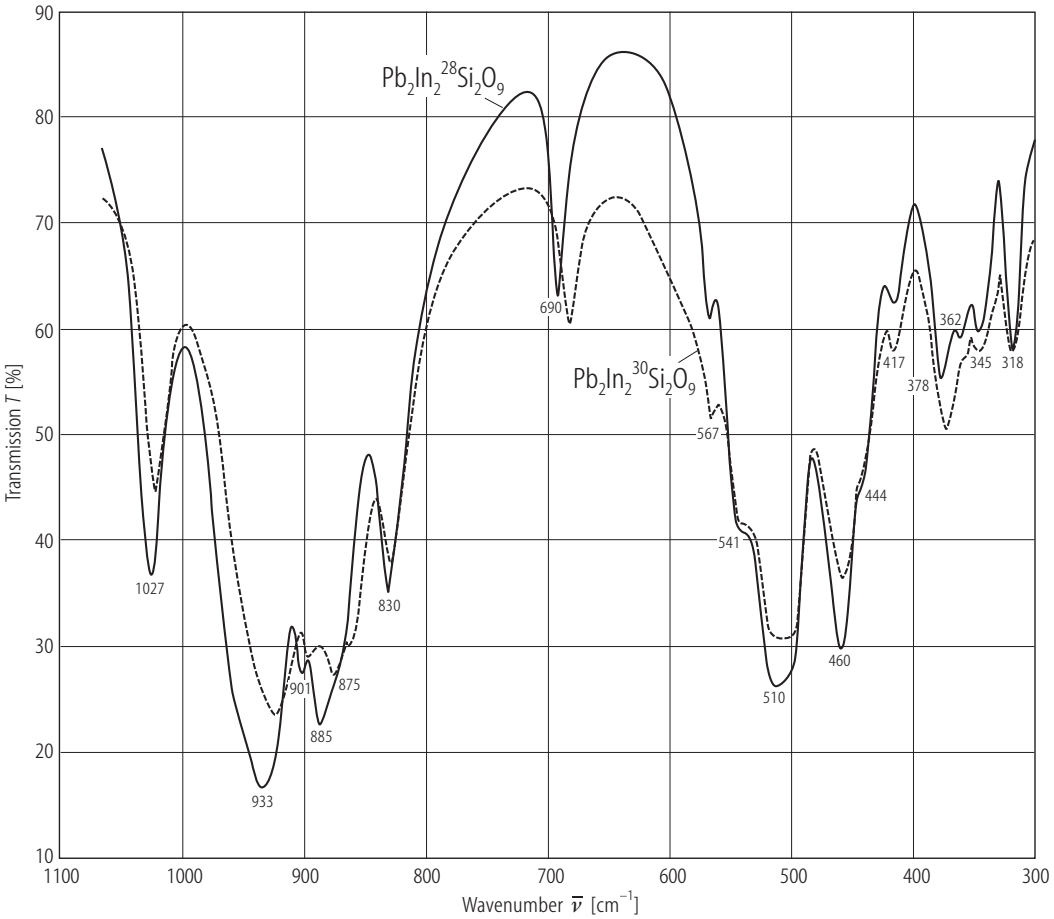

Fig. 6. $Pb_2In_2Si_2O_9$. Infrared spectrum showing the ^{28}Si–^{30}Si isotopic shifts. The frequency values are related to the ^{28}Si silicate [79G1].

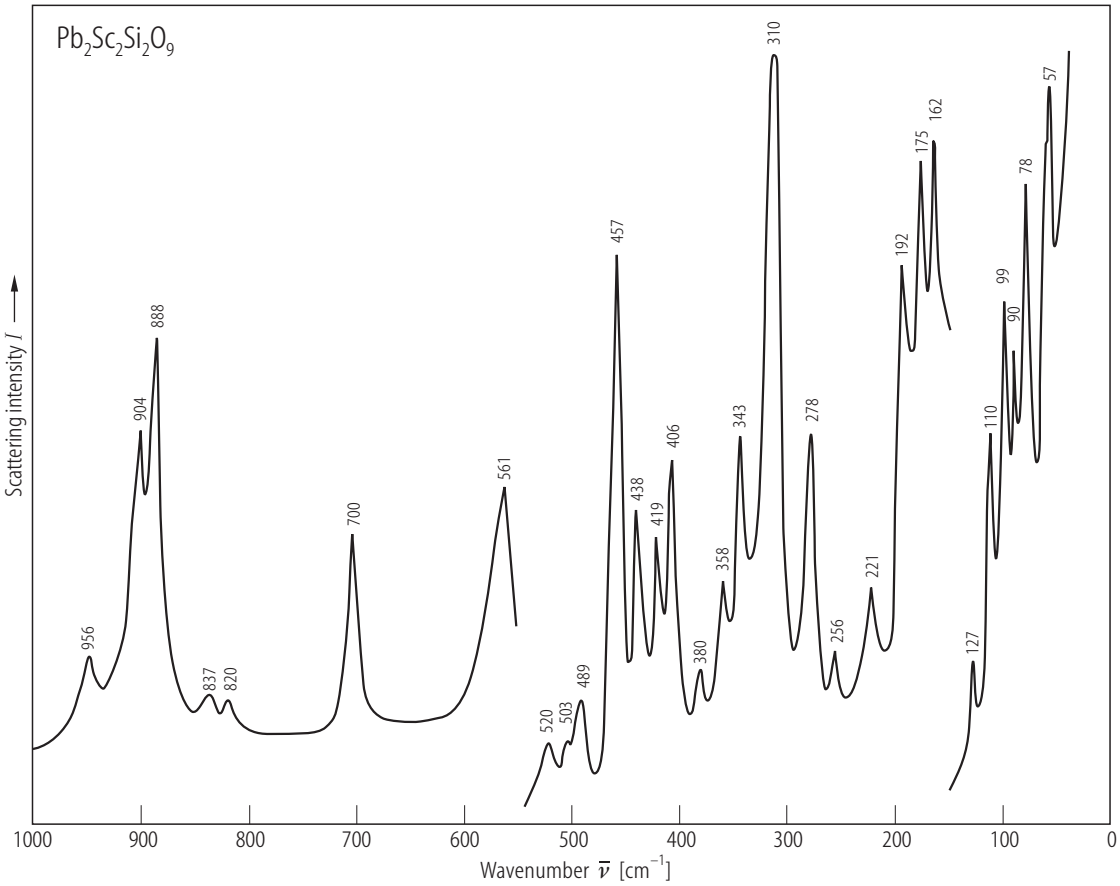

Fig. 7. $Pb_2Sc_2Si_2O_9$. Raman spectrum [79G1].

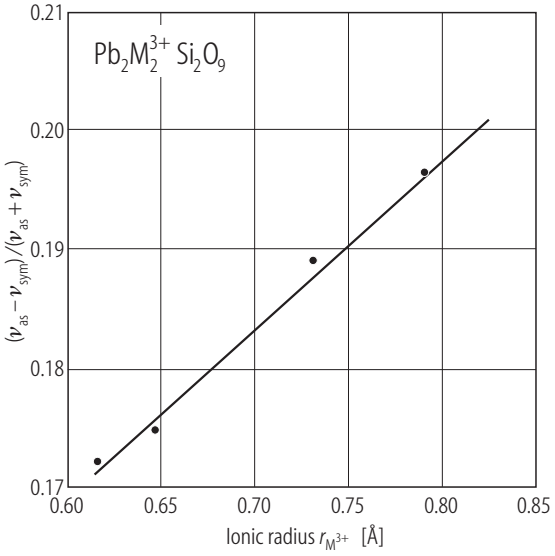

Fig. 8. Kentrolites $Pb_2M_2^{3+}Si_2O_9$. The ratio $(\nu_{as}-\nu_{sym})$ / $(\nu_{as}+\nu_{sym})$ as function of M^{3+} ionic radius[79G1].

References for 8.1.2.6

61K1 Kravchenko, S.M., Vlasova, E.V., Kazakova, M.E., Ilokhin, V.V., Abrashev, K.K.: Dokl. Akad Nauk SSSR 141 (1961) 1198
61W1 Watanabe, T., Takeuchi, Y., Ito, J.: Mineral. J. (Japan) 3 (1961) 159
62G1 Gabrielson, O.: Ark. Mineral. Geol. 3 (1962) 141
62G2 Gerasimovskii, V.I., Kazakova, M.E.: Dokl. Akad Nauk SSSR 142 (1962) 670
64W1 Woodrow, P.J.: Nature 204 (1964) 375
65K1 Khalilov, A.D., Mamedov, Kh.S., Makarov, E.S.: Dokl. Akad Nauk SSSR 161 (1965) 1409
65K2 Khalilov, A.D., Makarov, E.S., Mamedov, Kh.S.: Dokl. Akad Nauk SSSR 162 (1965) 179
66I1 Ito, J., Frondel, C.: Ark. Mineral. Geol. 4 (1966) 387
66K1 Khalilov, A.D., Makarov, E.S.: Geokhimiya 3 (1966) 256
67G1 Glasser, F.P.: Am. Mineral. 52 (1967) 1085
67W1 Woodrow, P.J.: Acta Crystallogr. 22 (1967) 673
68I1 Ito, J., Frondel, C.: Am. Mineral 53 (1968) 1276
68I2 Ito, J.: Am. Mineral. 53 (1968) 1663
69M1 Moore, P.B., Lousnathan, S.J.: Z. Kristallogr. 130 (1969) 438
71C1 Chernov, A.N., Ilyukhin, V.V., Maksimov, B.A., Belov, N.V.: Kristallografiya 16 (1971) 87 (Sov. Phys. Crystallogr. 16 (1971) 65)
71R1 Rastsvetaeva, R.K., Simonov, V.I., Belov, N.V.: Dokl. Akad Nauk SSSR 197 (1971) 81 (Sov. Phys. Dokl. 16 (1971) 182)
74K1 Kapustin, Yu.L., Khomyakov, A.P., Semenov, E.I., Eskova, E.M., Bykova, A.V., Pudovkina, Z.V.: Zap. Vses. Mineral. Ova. 103 (1974) 567
75M1 Menshikov, Yu.P., Bussen, I.V., Goiko, E.A., Zabavnikova, N.I., Merkov, A.N., Khomyakov, A.P.: Zap. Vses. Mineral. Ova. 104 (1975) 322
75R1 Rastsvetaeva, R.K., Sirota, M.I., Belov, N.V.: Kristallografiya 20 (1975)259 (Sov. Phys. Crystallogr. 20 (1975) 158)
76F1 Fleischer, M., Chao, G.Y., Mandarino, J.A.: Am. Mineral 61 (1970) 338
76O1 Olazcuaga, R., Le Flem, G., Hagenmüller, P.: Rev. Chim. Mineral. 13 (1976) 9
79G1 Gabelica-Robert, M., Tarte, P.: J. Solid State Chem. 27 (1979) 179
79K1 Keller, P., Dunn, P.J., Hess, H.: Neues Jahrb. Mineral. Monatsh. (1979) 203
80F1 Fleischer, M., Cabri, L.J., Pabst, A.: Am. Mineral. 65 (1980) 406
80H1 Hess, H., Keller, P.: Z. Kristallogr. 151 (1980) 287
80K1 Krutik, V.M., Pushcharovskii, D.Yu., Khomyakov, A.P., Pobedimskaya, E.A., Belov, N.V.: Kristallografiya 25 (1980) 240 (Sov. Phys. Crystallogr. 25 (1980) 138)
80W1 Williams, S.A., Duggan, M.: Bull. Mineral. 103 (1980) 530
81F1 Fleischer, M., Gabri, L.: Am. Mineral. 66 (1981) 637
82W1 Williams, S.A.: Mineral. Mag. 46 (1982) 363
83K1 Khomyakov, A.P., Kurova, T.A.,Chistyakova, N.I.: Zap. Vses. Mineral. Ova. 112 (1983) 456
83R1 Ronsbo, J.G., Lemardsen, E.S., Petersen, O.V., Johnsen, O.: Neues Jahrb. Mineral. Monatsh. (1983) 451
84D1 Dunn, P.J., Chao, G.J., Grice, J.D., Ferraido, J.A., Fleischer, M., Pabst, A., Zilczer, J.A.: Am. Mineral. 69 (1984) 565
84D2 Dunn, P.J., Fleischer, M., Francis, C.A., Langley, R.H., Kissin, S.A., Shigley, J.E., Vanko, D.A., Zilczer, J.A.: Am. Mineral. 69 (1984) 810
86R1 Rastsvetaeva, R.K.: Kristallografiya 31 (1986) 1070 (Sov. Phys. Crystallogr. 31 (1986) 633)
86R2 Rastsvetaeva, R.K., Adrianov, V.I.: Kristallografiya 31 (1986) 82 (Sov. Phys. Crystallogr. 31 (1986) 44)
89K1 Khalilov, A.D.: Mineral. Zh. 11 (1989) 19
90E1 Egorov-Tismenko, Yu.K., Sokolova, E.V.: Mineral. Zh. 12 (1990) 40
91M1 Moore, P.B., Sen Gupta, P.K., Shen, J., Schlemper, E.O.: Am. Mineral. 76 (1991) 1389
91N1 Nickel, E.H., Nichols, M.C.: Mineral Reference Manual, Van Nostrand Reinhold, 1991
00M1 Massa, W., Yakubovich, O.V., Kireev, V.V., Melnikov, O.K.: Solid State Sci. 2 (2000) 615.